Inorganic Chemistry

ARTICLE

pubs.acs.org/IC

Synthesis and Characterization of a Stable Bismuth(III) A_3−Corrole

Lorenz Michael Reith,[†] Martin Stiftinger,[‡] Uwe Monkowius,[†] Günther Knör,*[,†] and Wolfgang Schoefberger*[,†]

[†]Institute of Inorganic Chemistry and [‡] Institute of Analytical Chemistry, Johannes Kepler University Linz (JKU), Altenberger Strasse 69, A-4040 Linz, Austria

Supporting Information

ABSTRACT: An efficient metalation procedure for bismuth complexes with meso-substituted corrole ligands is presented. Reaction of 5,10,15-tris-pentafluorophenylcorrole H_3(TpFPC) with Bi{N($SiMe_3$)$_3$} converts the free ligand H_3(TpFPC) to a neutral low-valent species Bi(TpFPC), which has been characterized by different spectroscopic techniques. (Spectro)electrochemical studies were performed in order to describe the redox potentials of the Bi(TpFPC) complex and to ascribe the sites of electron transfer. The first crystal structure of a bismuth corrole is presented and compared to the geometry-optimized molecular structure obtained with density functional theory (DFT) calculations. We show an example of a 4-coordinate metallocorrole with a very large out-of-plane displacement and significant doming. The electronic structure of the novel bismuth corrole system is discussed in detail. Time-dependent DFT results support the proposed assignment of electronic transitions observed for the Bi(TpFPC) derivative. To account for the reactivity we investigated the photocatalytic properties of the Bi(TpFPC) complex.

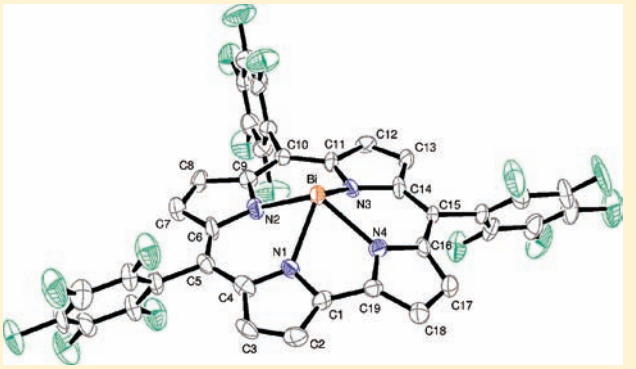

INTRODUCTION

Since the first published one-pot synthesis of corroles reported in 1999 by Gross and Paolesse,[1−3] the scope of corrole application grew tremendously including numerous examples of high-valent metallocorroles in the fields of catalysis, photochemical sensors, molecular electronics, and biomedicinal applications.[4]

In contrast to the corresponding porphyrin systems, free-base corroles show a considerably lower stability against light and air. This instability stems from the reduced aromaticity of corroles and the deformation of the macrocycle from planarity due to the steric bulk of the three interior hydrogens. Thus, corroles tend to break down to open chain structures in aerobic solution under ambient light.[5−7] Depending on the substitution pattern of the free-base corrole macrocycle the stability varies significantly, whereby those corroles bearing electronegative substituents display the highest stability compared to their counterparts bearing electropositive side groups. Nevertheless, corroles with electronegative substituents degrade at room temperature, under air, and ambient light. Barata et al. recently studied this process on the free-base 5,10,15-tris(pentafluorophenyl)corrole and observed slow oligomerization throughout the reaction processes.[8]

Despite this limited stability, many metalation reactions have to be performed under harsh conditions (e.g., boiling coordinating and noncoordinating solvents), and partial degradation reactions during the metalation process on the labile corrole macrocycle cannot be fully avoided. Moreover, for a few transition-metal and main-group metallocorroles no proper complexation procedure exists at present.

In comparison to the well-established synthetic routes for bismuth(III) porphyrins[9−13] and impressive derivatization procedures performed by Boitrel and co-workers, which were recently summarized in a review article,[14] only two examples of bismuth corrole complexes have been reported in the literature to date: bismuth octaethylcorrole Bi(OEC), which was prepared from H_3(OEC) with $BiCl_3$ and potassium acetate in boiling DMF for 20 min under inert atmosphere,[15] and recently, we reported a metalation reaction of H_3(TPC) with different bismuth salts in DMF and pyridine at elevated temperature.[16] Complexation reactions were indeed successful, but the obtained Bi(III) complexes lacked stability and demetalation occurred rapidly during purification. Similar results were obtained during the metalation of H_3(TPC) with Pb.[16,17] In order to overcome these obstacles and to prevent undesired degradation and side reactions by the use of gentle reaction conditions, we herein wish to report an efficient protocol for the synthesis of meso-substituted Bi(III)−corroles at room temperature.

SYNTHESIS

The free-base H_3(TpFPC), **2**, was synthesized by employing the condensation method for reactive aldehydes optimized by Gryko et al.,[18] where the solvent-free condensation of pyrrole and pentafluorobenzaldehyde is performed at room temperature under acidic catalysis followed by oxidation with DDQ. First attempts for the metalation of the free-base H_3(TpFPC), **2**,

Received: April 22, 2011
Published: June 13, 2011

dx.doi.org/10.1021/ic200840m | *Inorg. Chem.* 2011, 50, 6788–6797

Scheme 1. (a) Preparation of the $Bi\{N(SiMe_3)_2\}_3$, 1, Precursor, and (b) Synthesis of Bi(TpFPC), 3

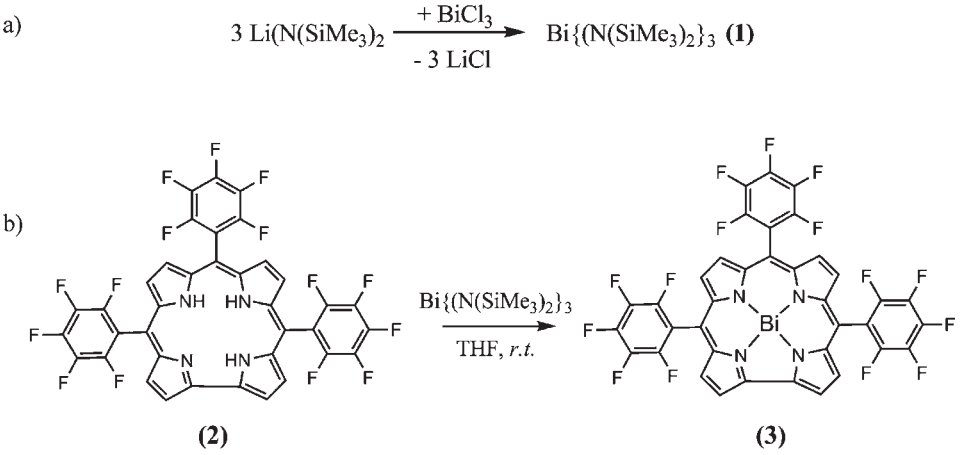

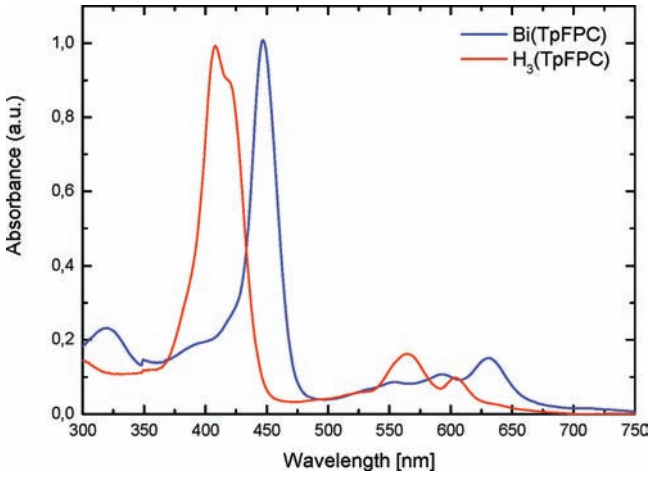

Figure 1. UV−vis absorption spectra of H_3(TpFPC), **2**, and Bi(TpFPC), **3**, in THF.

involved "standard" metalation procedures, which have been widely used for a variety porphyrins and corroles. Unfortunately, reactions of **2** with $BiCl_3$ in pyridine and DMF at elevated temperature were not successful, and the question of an alternative metalation method arose. Our interest soon focused on silyl−amide ligands which are versatile precursors for metalation agents[19] and easily accessible on a multigram scale starting from the commercially available starting materials $Li\{N(SiMe_3)_2\}$ or HMDS. Nevertheless, examples for application as a metalation agent for porphyrins and related macrocycles have mainly been limited to insertion of alkali metals,[20,21] and this strategy is unprecedented in the case of a corrole macrocycle.

Synthesis of the metalation agent $Bi\{N(SiMe_3)_2\}_3$, **1**, was achieved by reaction of $BiCl_3$ with $Li(N(SiMe_3)_2$ at −10 °C in abs. THF (illustrated in Scheme 1a).[22,23]

The preparation of Bi(TpFPC), **3**, from $Bi\{N(SiMe_3)_2\}_3$, **1**, and H_3(TpFPC), **2**, proved successful under mild conditions. In the following, the silyl amide **1** was dissolved in THF at room temperature and added dropwise to a solution of **2** in THF (Scheme 1b) under inert atmosphere. After workup the desired Bi(TpFPC) complex **3** could be isolated in 75% yield after column chromatography. Figure 1 indicates the bathochromic shift of the Soret (B) band in the UV−vis absorption spectrum in THF of Bi(TpFPC) compared to the free-base corrole H_3(TpFPC). Bi(TpFPC), **3**, exhibits no emission in ethanol at room temperature and at 77 K presumably due to radiationless intersystem crossing to a nonluminescent excited triplet state. As a consequence, in such a heavy atom macrocyclic system an increased triplet to singlet oxygen conversion is expected.

NMR SPECTROSCOPY

^{1}H NMR spectroscopy of Bi(TpFPC), **3**, in deuterated THF (Figure S3, Supporting Information) displayed the characteristic features for tris-pentafluorophenyl−corroles:[24] four doublets in the range between 8.5 and 9.1 ppm are observed with an integral of two protons each and coupling constants in the range of 4 Hz, typical for the 8 β-pyrrole protons.

Due to the symmetry of the Bi(TpFPC), **3**, molecule two sets of resonances can be observed with ^{19}F NMR spectroscopy (Figure 2): those for the fluorine atoms on the substituent on meso-positions 5 and 15 are chemically and magnetically equivalent and as such give rise to one set, and the fluorine atoms on the third meso-substituent (10) that give rise to the second set of resonances. Hence, two triplets are observed for the *para*-F atoms (around 157.5 ppm) with an integral ratio of 2:1. For each resonance, scalar couplings are only resolved to the two directly neighboring *meta*-F atoms ($^3J_{F-F} \geq 22$ Hz), while no $^4J_{F-F}$ couplings to the corresponding *ortho*-F atom are observable. Due to the nonplanarity of the bismuth corrole, an ABCDE spin system results. Therefore, four signals are observed for the *ortho*-F atoms with a 1:2:2:1 integral ratio, which means that within each of the pentafluorophenyl substituents the fluorine atoms above and those below the corrole plane are not chemically equivalent. This fact is also corroborated by analysis of the coupling pattern: all *ortho*-F resonances are observed as double doublets, with one $^3J_{F-F}$ coupling to the neighboring *meta*-F atom and an additional $^4J_{F-F}$ coupling of about 8 Hz. Having already excluded $^4J_{F-F}$ coupling between the *ortho*- and *para*-fluorine atoms, $^4J_{F-F}$ coupling between two *ortho*-F resonances seems to be the logical explanation for the observed coupling pattern.

Consequently, a 1:2:2:1 integral ratio is also observed for the *meta*-fluorine atoms, whereby two of the resonances are overlapping. Each *meta*-fluorine resonance is observed as an octet (ddd),

dx.doi.org/10.1021/ic200840m |*Inorg. Chem.* 2011, 50, 6788–6797

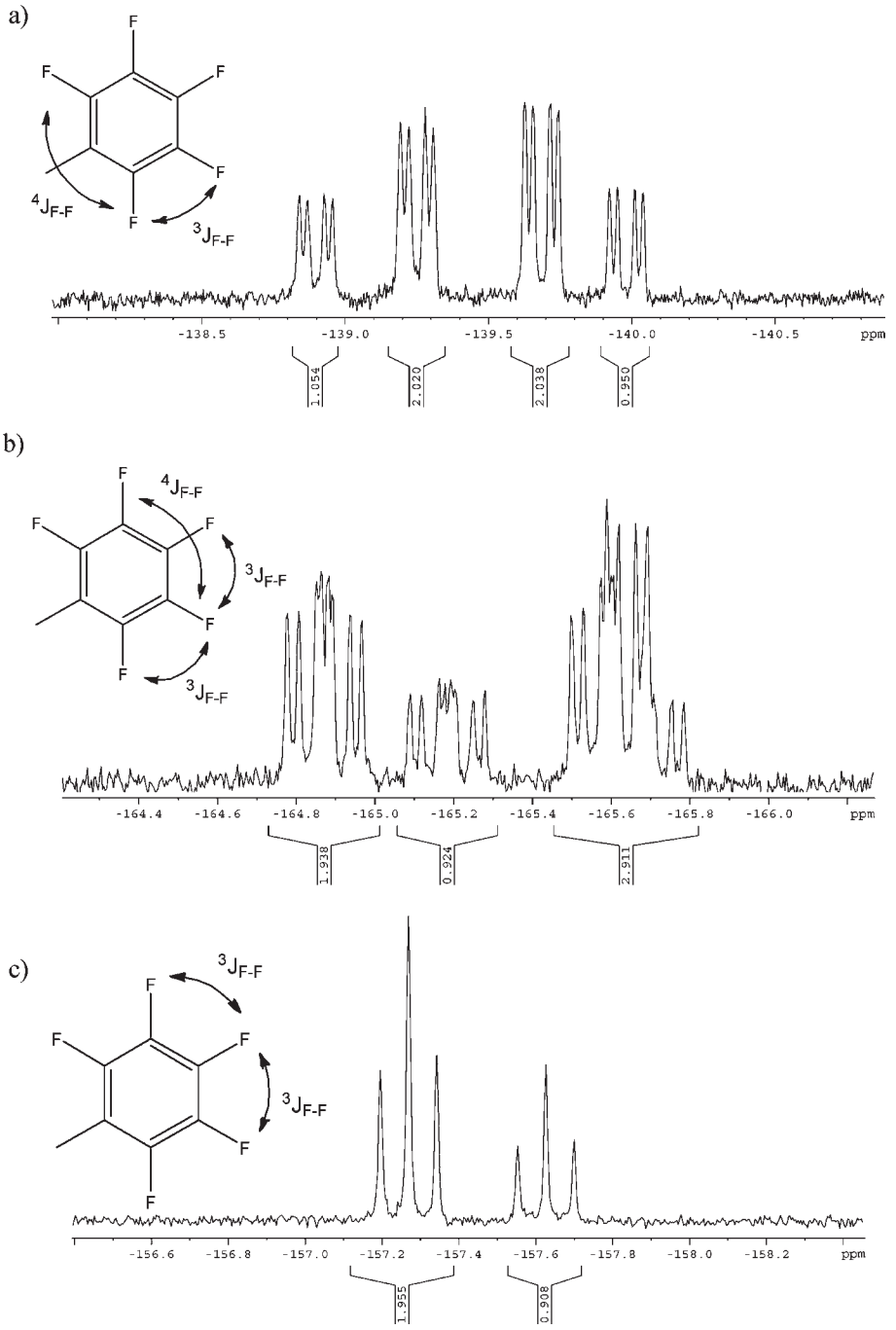

Figure 2. ^{19}F NMR spectrum of Bi(TpFPC) with schematic illustration of the observed couplings: (a) *ortho*-F region, (b) *meta*-F region, and (c) *para*-F region.

which is consistent with $^3J_{F-F}$ coupling to the corresponding neighbors in the ortho and para positions and $^4J_{F-F}$ to the second *meta*-fluorine atom on the same pentafluorophenyl ring.

In conclusion, Bi(TpFPC), **3**, does not only display a dome-featured structure (Figure 5b) in the solid state but also in solution, as clear differentiation between fluorine atoms above and below the corrole plane is possible.

■ ELECTROCHEMISTRY

Cyclic voltammetry (vs SCE) of **3** in acetonitrile with 0.1 mol of $TBAPF_6$ (Figure 3) reveals two consecutive oxidations at $E_{1/2}$ = 0.66 and 1.07 V that display reversibility (Figure 3a). The first reduction of **3** at $E_{1/2}$ = −1.28 V is also reversible, followed by a second irreversible reduction at $E_{1/2}$= −1.88 V (Figure 3b). The product of this second reduction shows reoxidation at −0.4 V. This pattern is similar to the electrochemical behavior of Bi(OEC), which shows oxidations at $E_{1/2}$ = 0.24 and 0.78 V and one single reduction at $E_{1/2}$= −1.74 V vs SCE.[15] While a higher potential for the oxidation of **3** is necessary, reduction is easier compared to Bi(OEC). This behavior can be attributed to the three pentafluorophenyl groups which have a strongly electron-withdrawing effect on the macrocycle, thus facilitating reduction

dx.doi.org/10.1021/ic200840m |*Inorg. Chem.* 2011, 50, 6788–6797

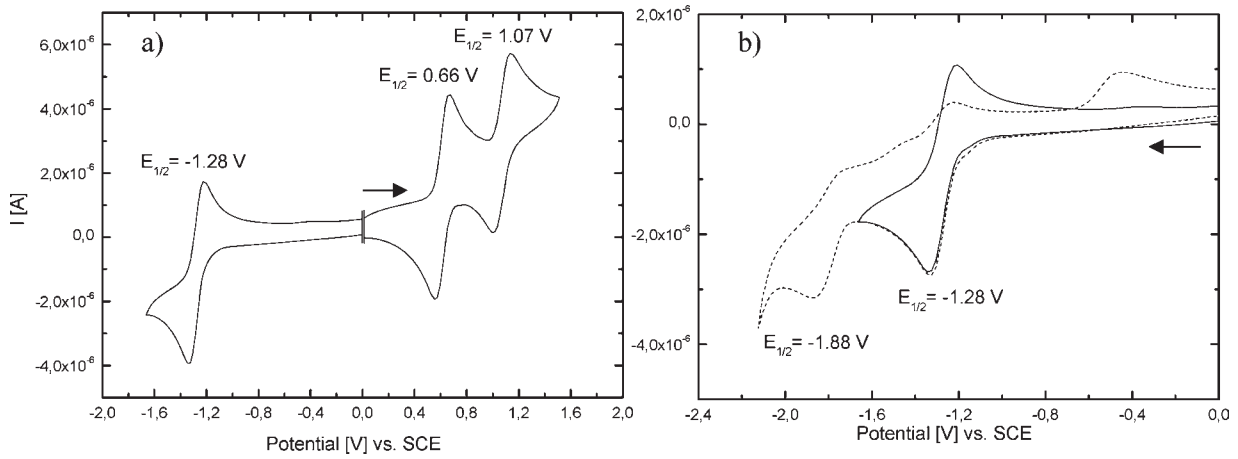

Figure 3. Cyclic voltammograms of Bi(TpFPC), **3**, in ACN with 0.1 M $TBAPF_6$ measured with a scanning rate of 50 mV/s: (a) electrochemical oxidation and reduction processes (overview) and (b) electrochemical reduction process.

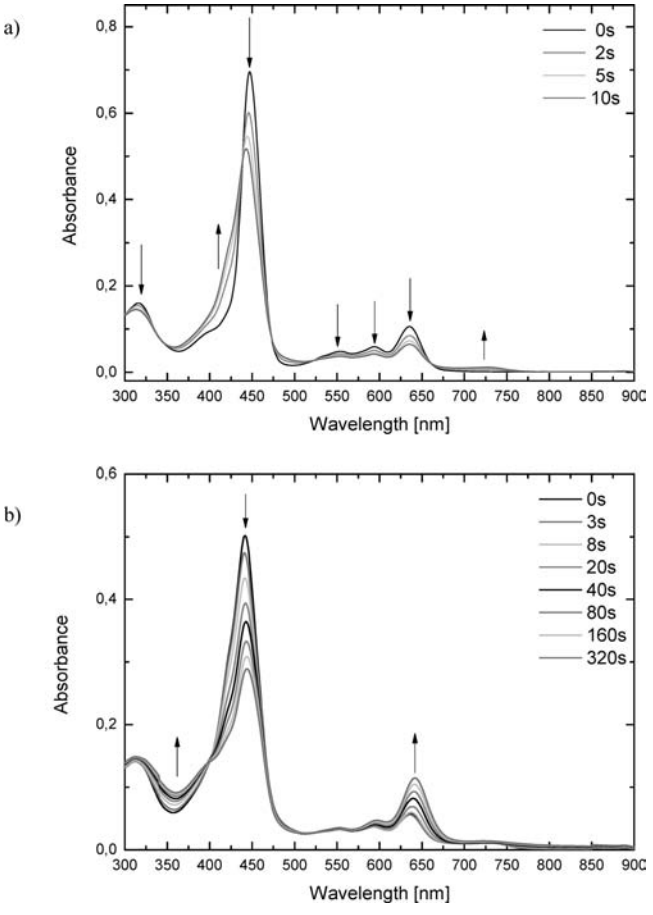

Figure 4. UV−vis absorption spectral changes during the electrochemical oxidation of Bi(TpFPC), **3**, in ACN with 0.1 M $TBAPF_6$ at (a) 0.77 and (b) 1.2 V.

and impeding oxidation, a trend which has already been observed for other pentafluorophenyl-substituted metallocorrole systems.[25]

Spectroelectrochemistry was performed in an optically transparent thin layer electrode OTTLE cell[26] in order to facilitate the assignment of the sites of electrochemical oxidations. Along with the first oxidation, the intensity of the Soret (B) band and the three Q bands decrease and a blue shift of the B band from 447 to 443 nm is observed (Figure 4a). During the second oxidation, the intensity of the B band is decreasing strongly while the intensity of the Q bands increases, and the most intense Q band shows a red shift from 635 to 643 nm (Figure 4b).

While metal-centered reduction of Bi(III) to Bi(II) species in porphyrinoid macrocycles has not yet been observed, it seems rather unlikely to be reversible due to the tendency of Bi(II) intermediates to undergo rapid disproportionation processes. As such, the first reduction can be assigned as a ring-centered process. Classification of the two reversible oxidations is not that straightforward. In our view, arguments in favor of two consecutive ring-centered reactions prevail: For the first oxidation, the situation seems to be very similar to Bi(OEC),[15] as for both derivatives a decrease of B and Q bands is observed and the spectrum of the oxidized form displays characteristics of a π-radical cation. In addition, abstraction of one of the Bi 6s electrons at a potential lower than for the TpFPC-macrocycle would be very atypical, especially regarding the strong inert pair effect of bismuth and the accompanying stabilization of the Bi(III) oxidation state.

For the second oxidation, spectroelectrochemistry also does not reveal any evidence for a metal-centered process. Consequently, formation of a corrolato dication species seems to occur, where a second electron is removed from the conjugated π-electron system. This means that, at least under the experimental conditions employed here, the two consecutive oxidations in **3** are ring-centered processes, which are comparable to the usual electrochemical oxidation behavior of different bismuth porphyrins reported earlier.[11]

X-RAY CRYSTALLOGRAPHY

Figure 5 illustrates ORTEP plots, representing X-ray crystal structures of the free-base corrole H_3(TpFC), **2**, and the metalated counterpart Bi(TpFPC), **3**. To our knowledge, complex **3** is the first bismuth corrole characterized by single-crystal X-ray diffraction. The crystallographic data are summarized in Table 1. The substances were found to crystallize in the monoclinic space groups $P2_1$ (**2**, Z = 2) and $P2_1/n$ (**3**, Z = 4) as chloroform solvates. Despite many decades of corrole research, only nine crystal structures of free-base triaryl corroles have been published according to a CSD query.[27−32] Among them, two crystal structures of the corrole **2** were reported, one containing *m*-xylene[3] and the other ethyl acetate.[6] Analogous to these two structures,

dx.doi.org/10.1021/ic200840m |*Inorg. Chem.* 2011, 50, 6788–6797

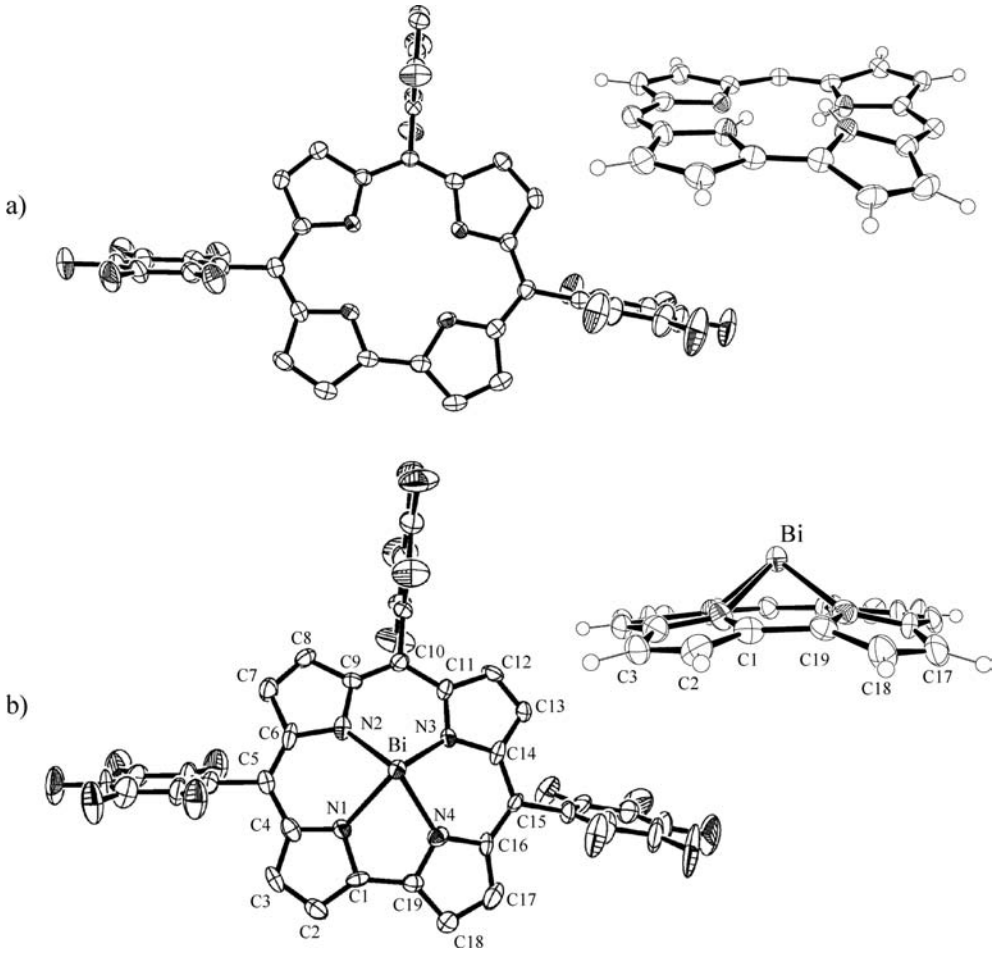

Figure 5. Molecular structures of (a) H_3(TpFPC), **2**, and (b) Bi(TpFPC), **3**. (Top views) ORTEP representations with atom labeling, thermal ellipsoids at 50% probability (H atoms omitted for clarity). (Inserts) Side views along the C1−C19 axis (meso substituents omitted for clarity).

the three NH protons can unambiguously be located on rings A, B, and D and the macrocylce is considerably distorted from planarity due to the steric repulsion of the inner protons.

Comparable to the published Bi(III)porphyrin structures,[14] the corrole macrocycle exhibits a dome-shaped structure and the bismuth atom lies ∼1.15 Å above the plane defined by the four nitrogen atoms of the corrole ring. The Bi atom is coordinated exclusively by the four nitrogen atoms and no evidence for axial coordination is found. By comparing the structure of the Bi(TpFPC), **3**, to other examples of main-group-metal corroles,[33] we show the first example of a 4-coordinate metallocorrole with the largest out-of-plane displacement and most significant doming of the macrocycle. The molecular geometry of Bi(TpFPC), **3**, was optimized by DFT calculation and indeed also resulted in a domed structure. An overlay of both structures is found in Figure S10, Supporting Information (detailed distances and dihedral angles are listed in Table 2). The out-of-plane displacement of the central bismuth ion, which differs by about 0.1 Å, and the calculated Bi−N distances as well as the dihedral angles $\chi_1 - \chi_4$, which are a measure of the doming of the macrocycle, are comparable for both structures. The geometry optimized structure slightly overestimates the doming effect, and the pyrrole moieties are slightly more bended, especially in the region of the direct pyrrole−pyrrole linkage. Additionally, in the crystal structure one of the pyrrole groups ($N_3-C_{11}-C_{12}-C_{13}-C_{14}-N_3$) is tilted more in the macrocyclic plane compared to the residual pyrrole moieties, which means that the mean N_4 plane is somewhat ill defined compared to the geometry-optimized structure. As a consequence of these two effects, the calculated structure leads to partially larger distances between the inner nitrogen atoms and a larger central cavity, which is, in the absence of axial ligands, the key factor for influencing the out-of plane displacement of the central Bi atom, explaining the discrepancy between calculated and measured out-of-plane displacement. To summarize, the optimized structure agrees well with the crystal structure, whereby the deviations outlined above might result from packing effects in the solid state.

Electronic Structure and Calculated Properties. Recently, we discussed the electronic spectra of Bi(TPC), which also can be adopted in a slightly modified form for Bi(TpFPC), **3**.[16] The UV−vis spectrum for Bi(TpFPC), **3** (Figure 1), is qualitatively reproduced by time-dependent density functional theory (TD-DFT) calculations, and the corresponding transitions are depicted in Figure S11, Supporting Information. A simplified molecular orbital diagram is shown in Figure 6 describing the possible intraligand ($\pi-\pi^*$), MLCT, and metal-centered (MC) transitions. For the latter, time-dependent DFT calculations confirm the presence of a significantly Bi(6s)-localized HOMO in the $\pi-\pi^*$ frontier orbital region (Figure 7c−f) of the corrole ligand and also correctly describe the occurrence of a metal-centered

dx.doi.org/10.1021/ic200840m |*Inorg. Chem.* 2011, 50, 6788–6797

Table 1. X-ray Crystal Data of Compounds 2 and 3

	H_3(TpFPC)	Bi(TpFPC)
formula	$C_{37}H_{11}N_4F_{15}$, 2 $CHCl_3$	$C_{37}H_8N_4F_{15}$, $CHCl_3$
M_W [g/mol]	1035.23	1121.82
cryst size [mm]	0.55 × 0.32 × 0.30	0.55 × 0.35 × 0.25
cryst syst	monoclinic	monoclinc
space group	$P2_1$	$P2_1/n$
a [Å]	14.816(2)	15.402(2)
b [Å]	10.282(1)	10.862(2)
c [Å]	14.887(2)	24.331(4)
α [deg]	90	90
β [deg]	118.435(4)	90.261(6)
γ [deg]	90	90
V [Å^3]	1994.3(4)	4070.5(11)
ρ_{ber} [mg cm^{-3}]	1.724	1.831
Z	2	4
μ [mm^{-1}]	0.54	4.63
T [K]	200	200
Θ range [deg]	2.5−25.0	2.3−23.7
λ [Å]	0.71073	0.71073
reflns collected	19 439	6159
unique reflns	3726	6159
obsd reflns [$I > 2\sigma(I)$]	3277	4469
parameter refined/restraint	577/0	551/0
abs corr	multiscan	multiscan
T_{min}, T_{max}	0.76/0.85	0.19/0.39
σ_{fin} (max/min) [e Å^{-3}]	0.29/−0.40	2.41/−2.03
R_1 [$I \geq 2\sigma(I)$]	0.038	0.062
wR_2	0.092	0.157
CCDC	821890	821891

(MC) *sp*-transition in the UV region (Figure S18, Supporting Information). In ethanol solution additional electronic transitions of Bi(TpFPC), **3**, occur in the 305−340 nm region (32 787−29 412 cm^{-1}). The calculated metal-centered (MC) sp and MLCT transitions at 315−338 nm occur from the HOMO and HOMO−1, HOMO−3, HOMO−4, HOMO−6 to the LUMO, LUMO+2, LUMO+3, LUMO+5, which exhibit high $p_{x,y}$-orbital character (Figure S18, Supporting Information).

Interpretation of the natural bond orbital (NBO) population analysis on the bismuth atom and the corresponding pyrrole nitrogens in Bi(TpFPC), **3**, reveals relatively small NBO charges of 1.914 e and −0.698 e, respectively. The significantly lower NBO charge compared to the previously studied Bi(TPC) (NBO charge of 2.517e) indicates that the Bi−N bonds have a larger covalent character.[34]

The HOMO and LUMO energy levels were calculated from the peak potentials of the first oxidation and reduction processes obtained from cyclovoltammetry (Figure 3), leading to energy values of the two states (E_{HOMO} = −5.06 eV and E_{LUMO}= −3.12 eV). The resulting HOMO and LUMO energy gap of Bi(TpFPC), **3**, obtained from the cyclovoltammogram matches reasonably well with those obtained from gas-phase TD-DFT ($\Delta_{HOMO-LUMO,CV}$ = 1.94 eV, $\Delta_{HOMO-LUMO,TD-DFT}$ = 2.12 eV, $\Delta_{HOMO-LUMO,UV-vis}$ = 1.96 eV).

The unique structural motif of Bi(TpFPC), **3** (Figure 5b), with the large out-of-plane displacement of the central Bi ion and the significant doming of the macrocycle might be responsible for the relatively small 1.94 V difference in redox potentials.

Table 2. Comparison of Selected Distance and Dihedral Angles of the X-ray Crystal Structure and the Geometry-Optimized Structure of Bi(TpFPC), 3

	Bi(TpFPC) crystal structure	Bi(TpFPC) geometry optimized
out-of-plane distance	1.15	1.05
Bi−N(1)	2.23(1)	2.21
Bi−N(2)	2.28(1)	2.21
Bi−N(3)	2.24(1)	2.21
Bi−N(4)	2.23(1)	2.21
N(1)−N(2)	2.77	2.77
N(2)−N(3)	2.85	2.89
N(3)−N(4)	2.74	2.77
N(4)−N(1)	2.55	2.55
N(1)−Bi−N(2)	75.9(3)	77.7
N(1)−Bi−N(3)	118.1(3)	122.3
N(1)−Bi−N(4)	69.8(3)	70.5
N(2)−Bi−N(3)	78.2(3)	81.6
N(2)−Bi−N(4)	118.8(3)	123.2
N(3)−Bi−N(4)	75.6(3)	77.7
χ_1 ($C_3-C_4-C_6-C_7$)	15.3	19.4
χ_2($C_8-C_9-C_{11}-C_{12}$)	3.6	3.9
χ_3 ($C_{13}-C_{14}-C_{16}-C_{17}$)	26.8	25.2
χ_4 ($C_{17}-C_{18}-C_2-C_3$)	7.4	1.3

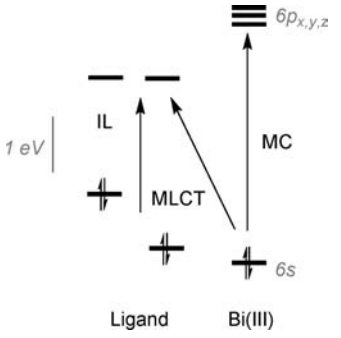

Figure 6. Qualitative MO diagram of Bi(TpFPC) **3**. IL: Intraligand ($\pi-\pi^*$) transitions involving electrons localized at the macrocyclic ring. MC: Metal-centered sp transitions. MLCT: Metal-to-ligand charge transfer.

CHEMICAL OXIDATION AND PHOTOCHEMISTRY

Chemical oxidation of Bi(TpFPC), **3**, with an excess of H_2O_2, iodosobenzene−diacetate, or $(NH_4)_2Ce(NO_3)_6$ was hampered by destruction of the macrocycle, while no evidence for the formation of higher valent bismuth−oxo species could be observed.

In order to photochemically oxidize Bi(TpFPC), **3**, to the corresponding Bi(V) species, as already demonstrated in the case of Bi(TPC),[16] Bi(TpFPC), **3**, was dissolved in ethanol and irradiated (λ > 455 nm) under aerobic conditions. Unlike Bi(TPC), where the high-valent state of bismuth could be reached via sensitization of the metal-centered sp excited states, mass spectrometry of the irradiated solution of **3** suggests formation of a

dx.doi.org/10.1021/ic200840m |*Inorg. Chem.* 2011, 50, 6788–6797

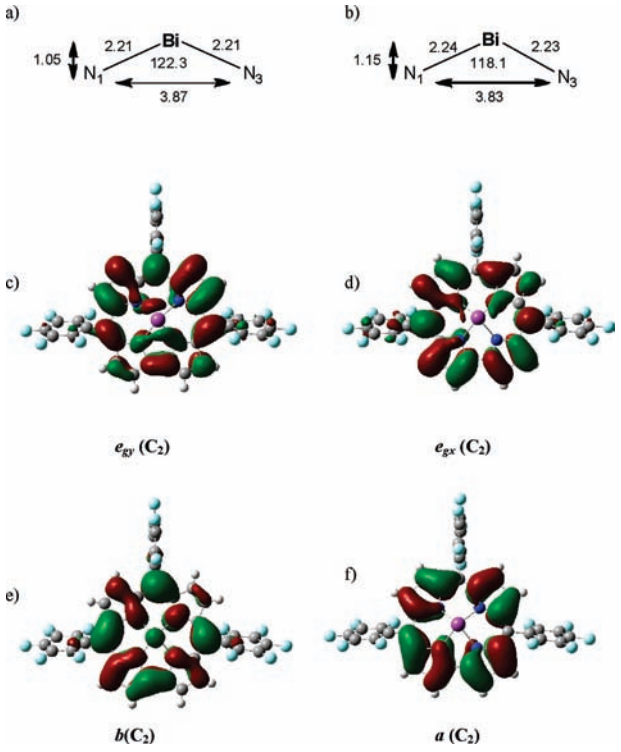

Figure 7. Comparison of structural parameters of the geometry-optimized structure (a) and the crystal structure (b) of Bi(TpFPC), **3**. Bond lengths and bond angles are indicated in the units of Ångstroms and degrees, respectively. The highest occupied molecular orbitals (HOMO, HOMO−1) and lowest unoccupied molecular orbitals (LUMO, LUMO+1) are depicted from c−f. A C_2 point group was assumed for Bi(TpFPC), **3**, and corresponds to a 2-fold rotational symmetry. The symmetry labels are added accordingly.

mixture of dioxo-open-chain structures (Figure S12b, Supporting Information), which also explains the UV−vis spectral changes during irradiation: new broad absorption bands between 360 and 380 as well as 520−670 nm with low intensity and a decrease of the characteristic B-band are observed (Figure S13, Supporting Information).

The strong −CH− to −C═O correlations observed in a long-range correlation $^{1}H-^{13}C$ HMBC spectrum, illustrated in Figure S14b, Supporting Information, supports our tentative assignment of the formation dioxo-open-chain tetrapyrrolic compounds.

Similar degradation products of iron corroles and porphyrins catalyzed by heme oxygenases have been presented recently. Nevertheless, additional ring-opening reactions at the meso-positions as reported by Świder et al. cannot be ruled out.[35]

Additionally, a Bi-peroxo species could be assigned with mass spectrometry as HOO−Bi(TpFPC) (m/z = 1035.03) (Figure S11, Supporting Information), which seems to represent an intermediate in the course of the degradation of **3**. This is supported by the fact that no accumulation of the HOO−Bi(TpFPC) species is observed upon longer irradiation time, while the amount of the open-chain product is growing constantly. Though it could not be proven unambiguously, axial ligation of Bi with the peroxo moiety would fit most logically into the reaction profile. In this context, it is interesting to note that similar metal−hydroperoxo species are discussed as critical intermediates formed in the course of heme−oxygenase-catalyzed tetrapyrrole ring cleavage.[36] These compound 0-type species represent an intermediate stage

Scheme 2. (a) Oxidation of Thioanisole Sensitized by Bi(TpFPC) (3), and (b) Singlet-Oxygen Ene (SOE) Reaction of Cyclohexene

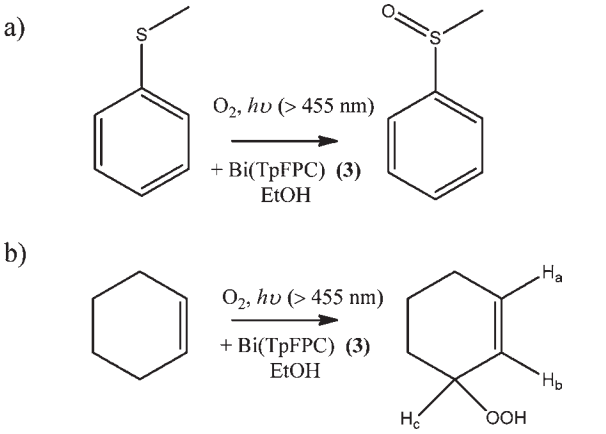

between dioxygen activation at the metal site and generation of high-valent oxo derivatives.[37] While this latter transformation was already observed for other bismuth corrole complexes,[16] in the case of **3** the bismuth(V) oxidation state seems to be inaccessible without decomposition.

Singlet Oxygen Formation. In order to evaluate the role of singlet oxygen generation sensitized by the low-valent complex Bi(TpFPC), **3**, irradiation experiments with different sensitizer concentrations in aerated ethanol solutions have been performed and compared with the reference photosensitizer Rose Bengal (φ_{Δ}= 0.68[38]) whereby 1,3-diphenylisobenzofurane (DPBF) was used as acceptor. Figure S14, Supporting Information, displays the concentration-dependent time course of the degradation compared with the reference sensitizer. To reassure the fact that singlet oxygen is the reactive species for decomposition of DPBF, control experiments with addition of NaN_3 were performed. Azide acts as quencher for the formed singlet oxygen, and thus, decomposition of DPBF should be slowed down with increasing azide concentration.[39] Indeed, as shown in Figure S15, Supporting Information, with increasing azide concentration degradation is slowed down by up to a factor of 7.

Application of Bi(TpFPC) as Photocatalyst for Selected Oxidation Reactions. Although a degradation reaction during irradiation was observed as outlined above, the potential of Bi(TpFPC), **3**, to act as photocatalyst was evaluated by means of the oxidation of thioanisole and cyclohexene with singlet oxygen. Both reactions are well suited for evaluation of photocatalysts and their mechanisms have been examined extensively.[40,41]

Oxidation of thioanisole with singlet oxygen (Scheme 2a) to methyl-phenyl-sulfoxide was evaluated and proved successful in ethanol under O_2 atmosphere, with a 1000-fold excess of the reactant over the photocatalyst. After 8 h of reaction time, nearly full conversion of the reactant was observed (Figure S16, Supporting Information) in a clean reaction, where neither nameable amounts of side products nor significant degradation of the catalyst was observed. Further oxidation of the sulfoxide to the sulfone was only observed in traces. Test reactions without catalyst or irradiation did not lead to detectable product formation.

Under similar conditions, oxidation of cyclohexene ("ene reaction") to the corrersponding allylic hydroperoxide (Scheme 2b) was examined and monitored via ^{1}H NMR spectroscopy (Figure S17, Supporting Information). In this case, only partial conversion

dx.doi.org/10.1021/ic200840m |*Inorg. Chem.* 2011, 50, 6788–6797

of the substrate to the desired product could be observed, accompanied by significant degradation of the catalyst within the 8 h of reaction time.

Similar to the photocatalytic reactions observed for antimony corroles, all evidence points towards singlet-oxygen as the exclusive oxidant in these reactions performed with Bi(TpFPC), **3**.

CONCLUSION

In the present work, we have shown the synthesis of Bi(III)-5,10,15-tris(pentafluorophenyl)corrole, Bi(TpFPC), **3**, using a novel procedure employing $Bi\{N(SiMe_3)_2\}_3$ as the metalation agent, which can be employed under very gentle conditions. The crystal structure of the complex exhibits considerable out-of-plane displacement of the central Bi atom and a slight out-of-plane bending of the corrole macrocycle. Geometry optimizations employing the density functional theoretical approach gave an almost identical structural motif and natural bond orbital (NBO−) analysis gave a central natural charge state of +1.914e, which means that Bi−N(C) bonds in the corrole complex possess a relatively large component of covalent bonding.

We found that with the selected corrole ligand system the first two electrochemical oxidation processes occur on the macrocyclic ring. Attempts for a chemical oxidation of the central bismuth(III) ion promptly resulted in demetalation and degradation of the corrole macrocycle.

Bi(TpFPC), **3**, displayed photocatalytic activity (λ > 455 nm) during oxidation of thioanisole and cyclohexene by singlet oxygen.

In order to broaden the scope of the presented metalation procedure and to study the substituent effect toward catalytic and photophysical properties, synthetic work on differently substituted Bi(III) A_3-corroles and Bi(III) A_2B-corroles is underway, as well as extension of the metalation procedure on other main-group metals.

MATERIALS AND METHODS

All chemicals were purchased from Sigma Aldrich or Acros Chemicals and used without further purification. Reagent-grade solvents were purchased from Fischer Chemicals and distilled prior to use. THF was distilled over sodium and benzophenone under an argon atmosphere and stored over molecular sieves (4 Å) upon use.

TLC was performed using Fluka silica gel (0.2 mm) on aluminum plates. Silica gel columns for chromatography were prepared with silica gel 60 (0.060−0.20 mesh ASTM) from Acros. Proton (^{1}H NMR) and carbon (^{13}C NMR) spectra were recorded on a Bruker DRX 500 spectrometer equipped with a cryogenically cooled probe (TXI) at 500 and 125.8 MHz, respectively, ^{19}F NMR spectra were recorded on a Bruker Avance 600 MHz or a Varian Inova 300 MHz spectrometer at 564.7 or 282.4 MHz. The chemical shifts are given in parts per million (ppm) on the delta scale (δ) and are referenced to TMS (δ = 0 ppm) for ^{1}H and TFA for ^{19}F. Mass spectra were collected on a Finnigan LCQ DecaXPplus Ion trap Mass spectrometer with ESI ion source, and MALDI-TOF measurements were collected with a Bruker Autoflex III Smartbeam spectrometer, whereby a matrix:sample ratio of 10:1 was used. High-resolution MS measurements were performed with a 6510 quadrupole/time-of-flight (Q-TOF) instrument (Agilent, Palo Alto, CA) using direct infusion of the sample solution at a flow rate of 40 μL/min by means of a model 22 syringe pump (Harvard Apparatus, South Natick, MA). UV−vis absorption spectra were measured on a Varian CARY 300 Bio spectrophotometer. All ε values are given in L mol^{-1}cm^{-1}.

Cyclic voltammetry was carried out under inert conditions in a glovebox (CV) using an Eco Autolab-type potentiostat with a self-made three-electrode cell consisting of a platinum working electrode, a platinum wire as a counter electrode, and a silver/silver-chloride pseudo-reference electrode. The materials were dissolved in acetonitrile with 0.1 M $TBAPF_6$ as the supporting electrolyte, and scanning rates of 50−200 mV/s were applied. Ferrocene was employed as internal standard for potential referencing, and the potentials were subsequently referenced vs SCE accordingly.[43]

Spectroelectrochemistry was performed in a thin layer OTTLE cell[26] with a platinum working electrode, a platinum wire as a counter electrode, and a silver reference electrode. The corresponding UV absorption spectra were collected with a Jasco V670 Spectrometer.

Singlet-Oxygen Assay. Evaluation of photosensitized singlet oxygen generation by Bi(TpfPC) was performed in ethanol solution at room temperature, whereby degradation of the $^1O_2$ scavenger (DPBF, 1,3-diphenylisobenzofurane) was monitored by the decline of the 411 nm absorption band. For all experiments the concentration of DPBF was adjusted to 150 μmol, and experiments with different sensitizer concentrations were performed. Rose Bengal was used as reference photosensitizer (φ_Δ= 0.68[38]) in a way that the absorbance of the main Q-band maximum of Bi(TpfPC) and the absorption maximum of rose Bengal were set to approximately identical values. After aeration of the samples, irradiation was performed with a 100 W high-pressure mercury lamp using a Schott GG 495 nm cutoff filter. As a control, no bleaching of DPBF occurred under anaerobic irradiation conditions.[44] For the control experiments, NaN_3 was additionally added in order to inhibit singlet oxygen formation.

Crystal Structure Determination. Crystals of **2** and **3**, mounted on a Mitegen Micromount, were automatically centered on a Bruker SMART X2S benchtop crystallographic system. Intensity measurements were performed using monochromated (doubly curved silicon crystal) Mo Kα radiation (0.71073 Å) from a sealed microfocus tube. APEX2 software was used for preliminary determination of the unit cell.[45] Determinations of integrated intensities and unit cell refinement were performed using SAINT.[46] Data were corrected for absorption effects with SADABS using the multiscan technique.[47] The structures were solved by direct methods (SHELXS-97)[48] and refined by full-matrix least-squares on F_o^2 (SHELXL-97).[48,49] The interior hydrogen atoms of **2** were located using the difference map and refined isotropically without restraint. All other H atoms were calculated geometrically, and a riding model was applied during the refinement process. Crystals of the Bi compound contain two molecules of chloroform, one of which is disordered. The disorder could not be resolved successfully. Hence, the program SQUEEZE,[50] a part of the PLATON package of crystallographic software, was used to calculate the solvent disorder area and remove its contribution to the overall intensity data.

DFT Calculations. All calculations were performed using the Gaussian 03 package version E02.[51] Electronic structure calculations were based on Kohn−Sham density functional theory (KS-DFT) with Becke's three-parameter hybrid functional (B3LYP)[52,53] and a compound basis set, where the Pople's 6-311+G(d,p) basis sets were used for C, H, N, F.[54,55]

For our system, we first performed a tight structural optimization, followed by a frequency calculation to confirm that the optimized structure was indeed a minimum (with no imaginary frequencies). Single-point frequency calculations and NBO analyses were carried out with tight SCF convergence and ultrafine grids in the structural optimizations.

Los Alamos National Laboratory 2 (LANL2) relativistic effective core potentials (RECPs)[56] were used to describe the core electrons of Bi atoms, and split-valence (double-ζ) basis sets were used to describe s- and p-valence electrons of Bi. The LANL2DZ basis set was augmented by adding one set of polarization functions on all atoms and one set of diffuse functions on all non-hydrogen atoms. To gain insight into the vertical singlet electronic states, time-dependent density functional theory[57] (TD-PBE0 method) calculations were performed. Energies reported herein

dx.doi.org/10.1021/ic200840m |Inorg. Chem. 2011, 50, 6788–6797

were evaluated using the fourth-order Møller−Plesset perturbation theory [MP4(SDQ)] in combination with PBE0 parametrization.

Synthesis of the Compounds. *Tris(bis(trimethylsilyl)amido)-bismuth $Bi\{N(SiMe_3)_2\}_3$ (**1**).* Synthesis in accordance to refs 22 and 23: 2.05 g (19.5 mmol) of $BiCl_3$ dissolved in 20 mL of THF were added dropwise to a solution of 3.27 g (6.5 mmol) of $LiN(SiMe_3)_2$ in 10 mL of THF at 10 °C under inert atmosphere. The solution was stirred for 3 h, during which the solution turned shimmering orange, followed by evaporation of the solvent. Subsequently, the residue was dissolved in pentane, filtered, and evaporated to dryness, yielding the pale yellow solid product. Analytical data are consistent with literature values[22] (2.31 g (3.34 mmol); 51.5% yield).

*Tris-Pentafluorophenylcorrole H_3(TpFPC) (**2**).* Synthesis in accordance to ref 18: 1.52 g (8 mmol) of pentafluorobenzaldehyde was mixed with 80 μL of a 10% TFA in CH_2Cl_2 and 840 μL (12 mmol) of pyrrole at 40 °C and vigorously stirred. After 10 min, 80 mL of CH_2Cl_2 and 2.2 g (9.6 mmol) of DDQ in 16 mL of THF/toluene 1:1 were added and stirred for further 5 min. Subsequently, the solution was passed over a chromatography column (silica; hexane:dichloromethane 2:1) and further purified by column chromatography using the same solvents (230 mg (0.288 mmol); 10.8% yield). Crystals suitable for single-crystal structure determination were obtained by slow evaporation of $CHCl_3$.

Complementary data: ^{1}H NMR (500 MHz, $CDCl_3$, 25 °C): δ = 9.10 (d, J = 4.1 Hz, 2H, H2 + H18), 8.76 (d, J = 4.5 Hz, 2H, H7 + H13), 8.55−8.60 (4H, 2d overlapping, H8 + H12 and H3 + H17). ^{19}F NMR (564.7 MHz, $CDCl_3$, 30 °C): −137.2 (2F), −137.7 (4F), −152.2 (2F), −152.7 (1F), −161.4 (4F), −161.9 (2F). MS (ESI$^-$): m/z calcd for $C_{37}H_{10}F_{15}N_4$, 795.07; found, 795.20 [M − H]$^-$. UV−vis (THF): λ_{max} = 408, 418(sh), 563, 604 nm.

*Bismuth tris-Pentafluorophenylcorrole Bi(TpFPC) (**3**).* Under N_2 atmosphere, 50 mg (0.063 mmol) of H_3(TpFPC) (**2**) was dissolved in 15 mL of abs. THF and 55 mg (0.078 mmol) of $Bi\{N(SiMe_3)_2\}_3$ dissolved in 2 mL of THF were added dropwise under permanent stirring. After 12 h at room temperature, during which the color of the reaction mixture changed from dark violet to dark green and the intense red fluorescence of the free-base corrole completely vanished (the reaction progress was followed with UV−vis spectroscopy), the solvent was evaporated and the crude product was purified with column chromatography (silica, hexane:dichloromethane 2:1) (45 mg (0.045 mmol); 71.3% yield).

^{1}H NMR (500 MHz, THF-d_8, 25 °C): δ = 9.12 (d, J = 4.1 Hz, 2H, H2 + H18), 8.91 (d, J = 4.0 Hz, 2H, H7 + H13), 8.63 (d, J = 4.1 Hz, 2H, H8 + H12), 8.49 (d, J = 4.0 Hz, 2H, H3 + H17). ^{19}F NMR (282.4 MHz, THF-d_8, 30 °C) δ = −138.9 (dd, ^3J = 24.3 Hz, ^4J = 8 Hz, 1F, Fo), −139.3 (dd, ^3J = 24.4 Hz, ^4J = 8.2 Hz, 2F, Fo), −139.6 (dd, ^3J = 24.9 Hz, ^4J = 8.2 Hz, 2F, Fo), −140.0 (dd, ^3J = 24.9 Hz, ^4J = 8 Hz, 1F, Fo), −157.3 (t, ^3J = 20.6 Hz, 2F, Fp), −157.6 (t, ^3J = 20.8 Hz, 1F, Fp), −164.9 (ddd, ^3J = 21.0 Hz, ^4J = 7.9 Hz, 2F, Fm), −165.2 (ddd, ^3J = 21.0 Hz, ^4J = 8.1 Hz, 1F, Fm), −165.6 (m, 3F, Fm). ^{13}C NMR (125.8 MHz, $CDCl_3$, 25 °C): δ = 116.8 (CH, 2C, C2 + C18), 126.3 (CH, 2C, C7 + C13), 122.5 (CH, 2C, C8 + C12), 121.5 (CH, 2C, C3 + C17). MS (MALDI): m/z calcd for $C_{37}H_8BiF_{15}N_4$, 1002.031; found (M$^+$), 1002.198. UV−vis (THF): $\lambda_{max}(\varepsilon)$ = 322 (21 300), 446 (112 300), 552 (5100), 591 (9200), 631 (14 200).

Reaction of O_2 with Thioanisole. 0.12 mL (1 mmol) of thioanisole and 1 mg (1 μmol) of **3** dissolved in 5 mL of ethanol under O_2 atmosphere were heated (60 °C) and simultaneously irradiated for 6 h with the light from a 150 W high-pressure mercury lamp (Heraeus Noblelight) filtered by a Schott GG 455 nm cutoff filter.

Reaction of O_2 with Cyclohexene. 0.1 mL (1 mmol) of cyclohexene and 1 mg (1 μmol) of **3** dissolved in 20 mL of ethanol under O_2 atmosphere were heated (60 °C) and simultaneously irradiated for 6 h with the light from a 150 W high-pressure mercury lamp (Heraeus Noblelight) filtered by a Schott GG 455 nm cutoff filter.

■ ASSOCIATED CONTENT

Supporting Information. This material is available free of charge via the Internet at http://pubs.acs.org.

■ AUTHOR INFORMATION

Corresponding Author

*Phone: +43-732-2468-8811 (W.S.); +43-732-2468-8800 (G.K.). E-mail: wolfgang.schoefberger@jku.at (W.S.); guenther.knoer@jku.at (G.K.).

■ ACKNOWLEDGMENT

Financial support of this work by the Austrian Science Fund (FWF project P18384 "Solid state and Liquid NMR of biomolecular Metalcomplexes" and FWF project P21045 "Bio-inspired Multielectron Transfer Photosensitizers") is gratefully acknowledged. We wish to thank Dr. Roland Fischer for valuable discussion and measurement of the ^{19}F NMR spectra.

■ REFERENCES

(1) Gross, Z.; Galili, N.; Saltsman, I. *Angew. Chem., Int. Ed.* **1999**, *38*, 1427.
(2) Paolesse, R.; Jaquinod, L.; Nurco, D. J.; Mini, S.; Sagone, F.; Boschia, T.; Smith, K. M. *Chem. Commun.* **1999**, 1307.
(3) Gross, Z.; Galili, N.; Simkhovich, L.; Saltsman, I.; Botoshansky, M.; Bläser, D.; Boese, R.; Goldberg, I. *Org. Lett.* **1999**, *1*, 599.
(4) Aviv-Harel, I.; Gross, Z. *Chem.—Eur. J.* **2009**, *15*, 8382.
(5) Geier, G. R.; Chick, J. F. B.; Callinan, J. B.; Reid, C. G.; Auguscinski, W. P. *J. Org. Chem.* **2004**, *69*, 4159.
(6) Ding, D.; Harvey, J. D.; Ziegler, C. J. *J. Porphyrins Phthalocyanines* **2005**, *9*, 22.
(7) Tardieux, C.; Gros, C. P.; Guilard, R. *J. Heterocycl. Chem.* **1998**, *35*, 965.
(8) Barata, J. F. B.; Graça, M.; Neves, P. M. S.; Tomé, A. C.; Amparo, M.; Faustino, F.; Silva, A. M. S.; Cavaleiro, J. A. S. *Tetrahedron Lett.* **2010**, *51*, 1537.
(9) Buchler, J. W.; Lay, K. L. *Inorg. Nucl. Chem. Lett.* **1974**, *10*, 297.
(10) Barbour, T.; Belcher, W. J.; Brothers, P. J.; Rickard, C. E. F.; Ware, D. C. *Inorg. Chem.* **1992**, *31*, 746.
(11) Michaudet, L.; Fasseur, D.; Guilard, R.; Ou, Z.; Kadish, K. M.; Dahaoui, S.; Lecomte, C. *J. Porphyrins Phthalocyanines* **2000**, *4*, 261.
(12) Boitrel, B.; Breede, M.; Brothers, P. J.; Hodgson, M.; Michaudet, L.; Rickard, C. E. F.; Salim, N. N. A. *Dalton Trans.* **2003**, 1803.
(13) Halime, Z.; Lachkar, M.; Roisnel, T.; Furet, E.; Halet, J.-F.; Boitrel, B. *Angew. Chem., Int. Ed.* **2007**, *46*, 5120.
(14) Lemon, C. M.; Brothers, P. J.; Boitrel, B. *Dalton Trans.* **2011**, DOI: 10.1039/c0dt01711f.
(15) Kadish, K. M.; Erben, C.; Ou, Z.; Adamian, V. A.; Will, S; Vogel, E. *Inorg. Chem.* **2000**, *39*, 3312.
(16) Reith, L. M.; Himmelsbach, M.; Schoefberger, W.; Knör, G. *J. Photochem. Photobiol. A: Chemistry* **2011**, *218*, 247.
(17) Schoefberger, W.; Lengwin, F.; Reith, L. M.; List, M.; Knör, G. *Inorg. Chem. Commun.* **2010**, *13*, 1187.
(18) Gryko, D. T.; Koszarna, B. *Org. Biomol. Chem.* **2003**, *1*, 350.
(19) Šimon, P.; Proft, F. d.; Jambor, R.; Růžička, A.; Dostál, L. *Angew. Chem., Int. Ed.* **2010**, *49*, 5468.
(20) Arnold, J.; Dawson, D. Y.; Hoffman, C. C. *J. Am. Chem. Soc.* **1993**, *115*, 27072713.
(21) Brand, H.; Capriotti, J. A.; Arnold, J. *Inorg. Chem.* **1994**, *33*, 4334.
(22) Vehkamäki, M.; Hatanpää, T.; Ritala, M.; Leskelä, M. *J. Mater. Chem.* **2004**, 3191.
(23) Carmalt, C. J.; Compton, N. A.; Errington, R. J.; Fisher, G. A.; Moenadar, I.; Norman, N. C. *Inorg. Synth.* **1997**, *31*, 98.

(24) Balazs, Y. S.; Saltsman, I.; Mahammed, A.; Tkachenko, E.; Golubkov, G.; Levine, J.; Gross, Z. *Magn. Reson. Chem.* **2004**, *42*, 624.
(25) Simkhovich, L.; Mahammed, A.; Goldberg, I.; Gross, Z. *Chem.—Eur. J.* **2001**, *7*, 1041.
(26) Krejčik, M.; Daněk, M.; Hartl, F. *J. Electroanal. Chem. Interfacial Electrochem.* **1991**, *317*, 179.
(27) Hiroto, S.; Hisaki, I.; Shinokubo, H.; Osuka, A. *Angew. Chem., Int. Ed.* **2005**, *44*, 6763.
(28) Gros, C. P.; Barbe, J. M.; Espinosa, E.; Guilard, R. *Angew. Chem., Int. Ed.* **2006**, *45*, 5642.
(29) Paolesse, R.; Marinia, A.; Nardisa, S.; Froiioa, A.; Mandoja, F.; Nurcob, D. J.; Prodic, L.; Montaltic, M.; Smith, K. M. *J. Porphyrins Phthalocyanines* **2003**, *7*, 25.
(30) Paolesse, R.; Nardis, S.; Venanzi, M.; Mastroianni, M.; Russo, M.; Fronczek, F. R.; Vicente, M. G. *Chem.—Eur. J.* **2003**, *9*, 1192.
(31) Du, R.; Liu, C.; Shen, D.; Chen, Q. *Synlett* **2009**, 2701.
(32) Kim, K.; Kim, I.; Maiti, N.; J.Kwon, S.; Bucella, D.; Egorova, O. A.; Lee, Y. S.; Kwak, J.; Churchill, D. G. *Polyhedron* **2009**, *28*, 2418.
(33) Aviv-Harel, I.; Gross, Z. *Coord. Chem. Rev.* **2011**, *255*, 717.
(34) Feng, X.; Yu, J.; Lei, M.; Fang, W.; Liu, S. *J. Phys. Chem. B* **2009**, *113*, 13381.
(35) Świder, P.; Nowak-Król, A.; Voloshchuk, R.; Lewtak, J. P.; Gryko, D. T.; Danikiewicz, W. *J. Mass. Spectrom.* **2010**, *45*, 1443.
(36) Montellano, P. R. O. D. *Acc. Chem. Res.* **1998**, *31*, 543.
(37) Karlin, K. D. *Nature* **2010**, *168−169*, 463.
(38) Packer, L.; Sies, H. *Singlet oxygen, UV-A and ozone*; Academic Press: San Diego, 2000.
(39) Hasty, N.; Merkel, P. B.; Radlick, P.; Kearns, D. R. *Tetrahedron Lett.* **1972**, *13*, 49.
(40) Ishiguro, K.; Hayashi, M.; Sawaki, Y. *J. Am. Chem. Soc.* **1996**, *118*, 7265.
(41) Kearns, D. R. *Chem. Rev.* **1971**, *71*, 395.
(42) Luobeznova, I.; Raizman, M.; Goldberg, I.; Gross, Z. *Inorg. Chem.* **2006**, 45.
(43) Pavlishchuk, V. V.; Addison, A. W. *Inorg. Chim. Acta* **2000**, *298*, 97.
(44) Kim, J. O.; Lee, Y.-A.; H.Yun, B.; Han, S. W.; Kwag, S. T.; Kim, S. K. *Biophys. J.* **2004**, *86*, 1012.
(45) *APEX2*, Version 2009.9 ed.; Bruker AXS Inc.: USA, 2009.
(46) Zhan, H. Y.; Liu, H. Y.; Chen, H. J.; Jiang, H. F. *Tetrahedron Lett.* **2009**, *50*, 2196.
(47) Sheldrick, G. M. *Program for absorption correction with the Bruker SMART system*, Version 2008/1 ed.; Universitat Göttingen: Germany, 1996.
(48) Sheldrick, G. M. *SHELXS-97*; University of Göttingen, Göttingen, Germany, 1997.
(49) Sheldrick, G. M. *Acta Crystallogr.* **2008**, *A64*, 112.
(50) Spek, A. L. *J. Appl. Crystallogr.* **2003**, *36*, 7.
(51) Frisch, M. J. et al. ; Gaussian, Inc.: Pittsburgh, PA, 2003.
(52) Lee, C.; Yang, W.; Parr, R. G. *Phys. Rev. B* **1988**, *37*, 785.
(53) Becke, A. D. *J. Chem. Phys.* **1993**, *98*, 5648.
(54) Krishnan, R.; Binkley, J. S.; Seeger, R.; Pople, J. A. *J. Chem. Phys.* **1980**, *72*, 650.
(55) Frisch, M. J.; Pople, J. A.; Binkley, J. S. *J. Chem. Phys.* **1984**, *80*, 3265.
(56) Wadt, W. R.; Hay, P. J. *J. Phys. Chem.* **1985**, *82*, 284.
(57) Casida, M. E.; Jaorski, C.; Casida, K. C.; Salahub, D. R. *J. Chem. Phys.* **1998**, *108*, 4439.